Technische Universität Ilmenau
Institut für Mathematik

Preprint No. M **15/03**

Mathematical model of vibrissae for surface texture detection

Joachim Steigenberger, Carsten Behn and Christoph Will

28. April 2015

Impressum:
Hrsg.: Leiter des Instituts für Mathematik
Weimarer Straße 25
98693 Ilmenau
Tel.: +49 3677 69-3621
Fax: +49 3677 69-3270
http://www.tu-ilmenau.de/math/

ilmedia

Mathematical model of vibrissae for surface texture detection

Joachim Steigenberger[*], **Carsten Behn**[†], and **Christoph Will**[†]

April 28, 2015

Abstract

The plane elastic bending rod serves as a model of biological and artificial vibrissae. One task of vibrissae is to scan surfaces in order to detect their textures. We sketch the theory of static bending rod problems with a view to this field of applications. The solutions of the respective autonomous boundary value problems are given analytically. Numerical simulations are done in some worked out examples. Being aware of the fact that (1) in papers, object detecting by means of touch is seemingly exclusively investigated under the assumption of ideal contact (no stiction or friction), and (2) our present omission of this assumption is based upon simplifying model properties, the conclusions give some corresponding discussions and proposals for improvements and necessary work in future.

Keywords: vibrissa, artificial sensor, surface detection.
MSC[2010]: 92C10, 74L15, 74K10

1 Introduction

A paragon of (biological or artificial) tactile sensors is the animal *vibrissa*, [Carl et al. 2012], [Voges et al. 2012]. This hair-like sensor serves for recognition and exploration of outer objects (existence, location, size, shape) by touching the objects' surfaces. The touch takes place in an *active mode* (vibrissa in an internally excited oscillating state, frequency disturbance owing to touch) or in a *passive mode* (vibrissa in rest-state, quasi-static deformation owing to touch). The perception (measuring?) of the effects is achieved by pressure- or strain-sensitive mechanoreceptors, [Behn and Steigenberger 2009], [Behn 2014], in the support region, their output signals are forwarded to the central nervous system for analysis.

In a corresponding theory, it is obvious to model the vibrissa by a thin elastic bending rod, supported in suitable way at its "lower" end, where the supporting device is equipped with certain elements for measuring (forces, torques, frequencies) or vibration excitation. The outer object is taken as a rigid or deformable solid body, the touch takes place at the tip of the rod or at some point between support and tip. The adequate mathematical model is based on the theory of the *Euler-Bernoulli bending rod* in $\mathbb{R}^2$, and the touching processes show up as ordinary boundary value problems of order three or four, [Will 2013]. Concrete dimensions of both vibrissa and outer object can be removed from the theory by suitable normalization.

Seemingly every theory presupposes an *ideal contact* vibrissa-object, [Scholz and Rahn 2004], [Clements and Rahn 2006], [Will et al. 2014a], [Will et al. 2014b], i.e., the contact force (reaction force to constraint "touch") is in normal direction to the contacting surfaces. Physically, this means smooth surfaces, an assumption which is a more or less crude approximation in any application. Therefore, it seems reasonable to allow for physical non-smoothness in dealing with tactile sensing.

[*]Institute of Mathematics, Ilmenau University of Technology, Weimarer Straße 25, 98693 Ilmenau, Germany
[†]Department of Technical Mechanics, Faculty of Mechanical Engineering, Ilmenau University of Technology, Max-Planck-Ring 12 (Building F), 98693 Ilmenau, Germany; carsten.behn@tu-ilmenau.de

As a first step, we give in the following a simple theoretical description of how to determine the "roughness" of a surface by means of a scan with an (artificial) vibrissa.

The trivial paragon for this approach is just the everyday procedure of roughly finding out the surface texture of something: scratch the surface with your finger-nail (keeping the nail's edge in movement direction) and observe the produced noise that may hint to a stick-slip motion. This scenario suggests to use a model like the following. A straight vibrissa is pressed against a horizontal plane object surface by means of a force (acting at the foot of the vibrissa) in normal direction to the plane. Thereby, the vibrissa gets bent such that its tip contacts the plane with inclination neither normal nor tangential, the equilibrating contact force is vertical. If the vibrissa foot is horizontally displaced then the vibrissa tip slides along the plane while the vibrissa undergoes a translation, if and only if the contact is ideal, else, if there is some "dry friction" then the tip is kept fixed by some horizontal counter-force until a certain threshold is exceeded. So, a stick-slip behavior of the vibrissa occurs that could be observed through registration of the forces in the vibrissa support, giving a qualitative or even quantitative statement about the surface texture.

The paper at hand presents a first theoretical penetration of this scenario. It was not planned as a mature one that achieves ultimate results. It is just to serve as a basic tool for investigations to come next.

As the authors are working in a multi-disciplinary research group (reaching from engineering and mathematics to zoology) it frequently happens that various irritations come up during discussions. That is why the present paper terminates with a Supplement (see Appendix B) which is hoped to clarify misunderstandings concerning investigation methods.

Sections which are dominated by purely mathematical content are marked by an asterisk *.

2 The Euler-Bernoulli bending rod

Under certain simplifying assumptions which fit our context we consider a rod of circular cylindrical original shape, that consists of Hooke material, deforms by bending in a plane, has a constant bending stiffness, and undergoes no stretching so that the arc-length s of the elastic line shows up as a parameter that is invariant w.r.t. deformation. One end of the rod is supposed to be clamped, at the other end there acts a (reaction or impressed) force. Every state of the rod is an equilibrium state, i.e., any change of state must be seen as a *quasistatic* one (no inertia effects). Details are shown in Figure 1.

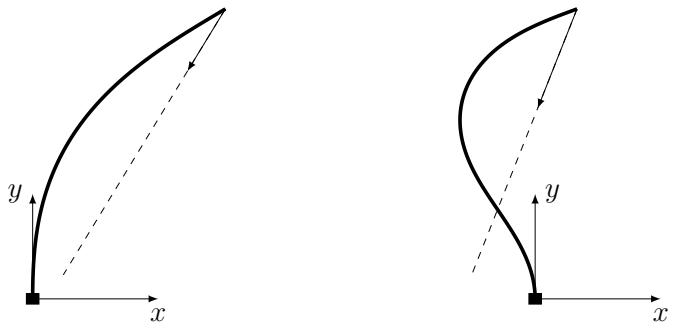

Figure 1: The deformed rod, two different states: $\alpha = -\frac{\pi}{6}$ (left), $\alpha = -\frac{\pi}{10}$ (right).

Possible or necessary relaxations of the postulated properties of the rod are discussed at the end of the paper.

Let the force be described as

$$\mathbf{f} = f_x\,\mathbf{e}_x + f_y\,\mathbf{e}_y\ ,$$
$$f_x = f\cdot\sin(\alpha),\quad f_y = -f\cdot\cos(\alpha),\quad f := \mid \mathbf{f} \mid,\ \alpha \in \left[-\tfrac{\pi}{2}, 0\right]\ .$$

(The restriction of α matches the applications to come; it might be changed on the spot.)
Generally, every geometric or physical quantity shall appear as a real number emerging from the following <u>normalization</u> (i.e., choice of *measuring units related to the actual system*) that rids the formalism of ballast and makes the results independent of the real system dimensions:

$$\boxed{\text{units:}\quad [\text{length}]=\mathrm{L}\ ;\ \ [\text{force}]=\mathrm{E\,I}_z\,\mathrm{L}^{-2}\ ;\ \ [\text{moment}]=\mathrm{E\,I}_z\,\mathrm{L}^{-1}\,,}$$

where L is the real length of the rod, E the elasticity modulus of the rod, and EI_z its constant bending stiffness. (In this formulation the rod has now length 1.)
Describe the elastic line of the deformed rod as $s \mapsto (x(s), y(s))$, $s \in [0,1]$, $s \mapsto \varphi(s)$ its slope. The static bending moment then writes

$$\begin{aligned} m(s) &= f_y\,\big(x_1 - x(s)\big) - f_x\,\big(y_1 - y(s)\big) \\ &= f \cdot \big\{\big(x(s) - x_1\big)\,\cos(\alpha) + \big(y(s) - y_1\big)\,\sin(\alpha)\big\}\ . \end{aligned}$$

The clamping reaction moment then is

$$m_0 = -m(+0) = f\,\{x_1\cos(\alpha) + y_1\sin(\alpha)\}\ .$$

Let $\kappa = \varphi'$ be the actual curvature of the deformed rod, then the central bending relation is $m = \kappa$, so the elastica is governed by the ordinary differential equations ($x' := \frac{dx}{ds}$, etc.)

$$\left.\begin{aligned} x' &= \cos\big(\varphi(s)\big)\,, \\ y' &= \sin\big(\varphi(s)\big)\,, \\ \varphi' &= f \cdot \big\{\big(x(s) - x_1\big)\,\cos(\alpha) + \big(y(s) - y_1\big)\,\sin(\alpha)\big\}\ , \end{aligned}\right\} \tag{2.1}$$

together with the boundary conditions

$$\left.\begin{aligned} x(0) &= 0, \quad & x(1) &= x_1, \\ y(0) &= 0, \quad & y(1) &= y_1, \\ \varphi(0) &= \tfrac{\pi}{2}, \quad & \varphi(1) &=: \varphi_1\,. \end{aligned}\right\} \tag{2.2}$$

The values in the right column may or may not be given in advance, nevertheless the tip coordinates x_1 and y_1 enter the differential equation. Anyway, this problem of order three has to be tackled as one packet.
We use a little trick by adding κ as another variable, whose derivative is known as $m' = f \cdot \{\cos(\varphi)\,\cos(\alpha) + \sin(\varphi)\,\sin(\alpha)\}$, coming up with a fourth order problem

$$\boxed{\begin{array}{lll} (a)\ \ x' = \cos\big(\varphi(s)\big), & (0)\ \ x(0) = 0, & (1)\ \ x(1) = x_1, \\ (b)\ \ y' = \sin\big(\varphi(s)\big), & (0)\ \ y(0) = 0, & (1)\ \ y(1) = y_1, \\ (c)\ \ \varphi' = \kappa(s), & (0)\ \ \varphi(0) = \tfrac{\pi}{2}, & (1)\ \ \varphi(1) = \varphi_1, \\ (d)\ \ \kappa' = f \cdot \cos\big(\varphi(s) - \alpha\big), & (0)\ \ \kappa(0) = m_0, & (1)\ \ \kappa(1) = 0\,. \end{array}} \tag{2.3}$$

Despite the raised order there are some advantages: none of the (possibly unknown) boundary values enters the differential equation anymore and, more important, the last two lines decouple from the upper ones forming a boundary value problem of order two per se. Moreover, the latter generates a useful first integral which is a step towards a formal solution.
Having in mind the scenario sketched in the Introduction it makes sense to restrict the tip angle φ_1 in all that follows:

$$0 \le \varphi_1 \le \frac{\pi}{2}\,.$$

Concerning α, we should envisage $\alpha = 0$ as starting value: the tip force $\mathbf{f}$ points vertically downward, causing a clamp reaction moment $m_0 > 0$. Then α takes negative values letting $\mathbf{f}$ rotate clockwise. Incidentally, $\mathbf{f}$ points to the clamp yielding $m_0 = 0$ while afterwards $\mathbf{f}$ will tend to some point $s^\flat > 0$ so as $m(s^\flat) = \kappa(s^\flat) = 0$. Altogether, it means, at $s^\flat$ the elastica has a *flex point* (curvature changing sign),

$$\kappa(s) \gtrless 0 \quad \text{iff} \quad s \lessgtr s^\flat\,.$$

2.1 Treating the mathematical model *

The ODEs (c) and (d) in (2.3), considering (c.1) and (d.1), generate the first integral

$$\boxed{\tfrac{1}{2}\kappa^2 = 2\,f\,\{\sin(\varphi-\alpha)-\sin(\varphi_1-\alpha)\}\,.} \tag{2.4}$$

This can be utilized in the sequel as a differential equation

$$\varphi'^2 = 2\,f\,[\sin(\varphi-\alpha)-\sin(\varphi_1-\alpha)]$$

for $\varphi(s)$ alone. But, to get φ' by taking the root, one has to take care of the sign because it rules the curvature behavior of the elastic line.

Anyway, φ'^2 has to be non-negative. Now, f is positive, and one may verify that with $\alpha \in [-\frac{\pi}{2}, 0]$ the bracket in (2.4) is non-negative if

$$0 \le \varphi_1 \le \frac{\pi}{2} + 2\,\alpha\,. \tag{2.5}$$

The meaning of the upper bound will become clear later on.

Hint: In the following, various integrals of elliptic type will appear. They can be represented by standard elliptic integrals which are handled on the computer. These representations are listed in the Appendix A and are frequently taken over from there.

2.1.1 Convex elastica

Assuming, inspired by Fig. 1(left), the *elastica as a right-handed curve* (negative curvature) it follows

$$\varphi' = -\sqrt{2f}\sqrt{\sin(\varphi-\alpha)-\sin(\varphi_1-\alpha)} =: \varkappa(\varphi; f, \varphi_1, \alpha). \tag{2.6}$$

Negative φ' makes $\varphi(s)$ monotonically decrease from $\frac{\pi}{2}$ to φ_1. So, we have $-\frac{\pi}{2} \le \alpha \le 0$ and $\varphi_1 \le \varphi \le \frac{\pi}{2}$. If we focus on the scenario sketched in the Introduction, then φ_1 must not be negative, and with (2.5) a non-negative radicand in (2.6) is guaranteed.

The differential equation for φ, $\varphi' = \varkappa(\varphi; f, \varphi_1, \alpha)$ contains f, φ_1, α as parameters. Together with the condition (c.0) in (2.3) separation of variables yields the solution

$$\sqrt{2f}\,s = -\int_{\frac{\pi}{2}}^{\varphi} [\sin(t-\alpha)-\sin(\varphi_1-\alpha)]^{-1/2}\,dt.$$

This integral can be rewritten with the help of standard elliptic integrals, at the moment it suffices to see it as a well-defined function K of $(\varphi, \varphi_1, \alpha)$. Therefore, the *central equation governing the elastica* is

$$\boxed{\begin{aligned} &\sqrt{2f}\,s = K(\varphi,\varphi_1,\alpha) := -\int_{\frac{\pi}{2}}^{\varphi} [\sin(t-\alpha)-\sin(\varphi_1-\alpha)]^{-1/2}\,dt, \\ &s \in [0,1], \quad \varphi \in \left[\varphi_1, \tfrac{\pi}{2}\right], \quad \varphi_1 \in \left[0, \tfrac{\pi}{2}+2\alpha\right]. \end{aligned}} \tag{2.7}$$

A crucial conclusion follows with $s = 1$, $\varphi(1) = \varphi_1$:

$$\boxed{f = \tfrac{1}{2}K^2(\varphi_1,\varphi_1,\alpha) =: f(\alpha,\varphi_1).} \tag{2.8}$$

This relates the acting force and the tip slope of the elastica. In the next Subsection 2.1.2, Fig. 2 gives an interesting sketch and a discussion of this relation.

The central equation above presents several different options to proceed towards the finally interesting function $s \mapsto (x(s), y(s))$.

(a) Since $K(\cdot,\varphi_1,\alpha)$ is monotonic, the central equation can be solved for φ (possible by using Jacobi functions). Then we had $\varphi = \Phi(s;f,\varphi_1,\alpha)$ to be put into the first two differential equations in (2.3), whence the elastica representation $s \mapsto (x(s),y(s))$ follows by integration.

(b) If we knew the parameters f,φ_1,α, then we could try to construct an approximate solution. To this end, one had to choose a finite sequence of (s,φ)-values in $[0,1]\times[\varphi_1,\frac{\pi}{2}]$ which solve the central equation. Then a suitable computer routine yields a polynomial $\varphi = pol(s)$ that interpolates or approximates the respective point sequence in the $(s,\varphi)-$plane. The rest is as in **(a)**.

(c) A general procedure is to consider the differential equations (2.3),(a),(b),(c). Since the central equation told us the monotonicity of $s \mapsto \varphi(s)$, this function can be used as a feasible parameter transformation on the elastica. Then, combining (a),(c) and (b),(c), we have (abusing notation) $x' = \frac{dx}{d\varphi}\,\varphi'$ and $y' = \frac{dy}{d\varphi}\,\varphi'$, and, with $\varphi' = \varkappa$, see (2.6), we get the transformed differential equations and initial conditions

$$\begin{aligned} \tfrac{dx}{d\varphi} &= \cos(\varphi)/\varkappa(\varphi;f,\varphi_1,\alpha), \quad x\left(\tfrac{\pi}{2}\right) = 0,\\ \tfrac{dy}{d\varphi} &= \sin(\varphi)/\varkappa(\varphi;f,\varphi_1,\alpha), \quad y\left(\tfrac{\pi}{2}\right) = 0. \end{aligned} \tag{2.9}$$

By integration we get the functions whose graph is the elastic line:

$$\boxed{\begin{aligned} x = X(\varphi;f,\varphi_1,\alpha) &:= \tfrac{-1}{\sqrt{2f}} \int_{\frac{\pi}{2}}^{\varphi} \cos(t)\,[\sin(t-\alpha)-\sin(\varphi_1-\alpha)]^{-1/2}\,dt,\\ y = Y(\varphi;f,\varphi_1,\alpha) &:= \tfrac{-1}{\sqrt{2f}} \int_{\frac{\pi}{2}}^{\varphi} \sin(t)\,[\sin(t-\alpha)-\sin(\varphi_1-\alpha)]^{-1/2}\,dt. \end{aligned}} \tag{2.10}$$

If a feasible triplet (f,φ_1,α) is given, then we are done, else the functions X and Y undergo further conditions (most important one in our scenario: fixed height $\eta < 1$ of the tip, i.e., $Y(\varphi_1;f,\varphi_1,\alpha) = \eta$). Again, these integrals can be rewritten with the help of standard elliptic integrals (see Appendix A), for the moment we will proceed with these functions X and Y taking them as given.

2.1.2 Elastica with one flex point

Now we assume, inspired by Fig. 1(right), that the elastica has one flex point $(x^\flat,y^\flat)$ at $s^\flat \in (0,1)$. Then (2.6) turns into

$$\varphi' = \begin{cases} \sqrt{2f}\sqrt{\sin(\varphi-\alpha)-\sin(\varphi_1-\alpha)} = -\varkappa(\varphi;f,\varphi_1,\alpha), & s < s^\flat,\\ -\sqrt{2f}\sqrt{\sin(\varphi-\alpha)-\sin(\varphi_1-\alpha)} = \varkappa(\varphi;f,\varphi_1,\alpha), & s > s^\flat. \end{cases} \tag{2.11}$$

If we put $\varphi(s^\flat) := \varphi^\flat > \frac{\pi}{2}$ (φ *increases* on $[0,s^\flat]$ from $\frac{\pi}{2}$ to $\varphi^\flat$ since φ' is non-negative), then there holds $\sin(\varphi^\flat-\alpha)-\sin(\varphi_1-\alpha) = 0$ and we get a relation between these angles

$$\varphi^\flat + \varphi_1 = \pi + 2\alpha. \tag{2.12}$$

This relation entails a nice conclusion concerning the angle $\varphi^\flat$. Since we are interested in vibrissae constrained by the horizontal plane $y = \eta$, we always have $\varphi_1 \in [0,\frac{\pi}{2}]$. This implies

$$\frac{\pi}{2} < \varphi^\flat \le \pi + 2\alpha \quad \text{and} \quad -\frac{\pi}{4} \le \alpha \le 0. \tag{2.13}$$

The integration in (2.11) which leads to the *central equation* has now to be done piecewise:

$$\begin{aligned} s < s^\flat: \qquad \sqrt{2f}\,s &= -\int_{\frac{\pi}{2}}^{\varphi} \tfrac{1}{\varkappa(\varphi;f,\varphi_1,\alpha)}\,d\varphi,\\ s > s^\flat: \quad \sqrt{2f}\,(s-1) &= \int_{\varphi_1}^{\varphi} \tfrac{1}{\varkappa(\varphi;f,\varphi_1,\alpha)}\,d\varphi, \end{aligned}$$

or for short

$$\boxed{\begin{array}{lll} \sqrt{2f}s & = -K(\varphi,\varphi_1,\alpha), & \varphi \in \left[\frac{\pi}{2},\varphi^\flat\right], \\ \sqrt{2f}(s-1) & = K(\varphi,\varphi_1,\alpha) - K(\varphi_1,\varphi_1,\alpha), & \varphi \in [\varphi_1,\varphi^\flat], \\ & & \text{with } \varphi^\flat = \pi + 2\alpha - \varphi_1. \end{array}} \tag{2.14}$$

(For $K(\cdot,\cdot,\cdot)$ remind (2.7).)

Putting $s = s^\flat$, $\varphi = \varphi^\flat$, we obtain $\sqrt{2f}\, s^\flat = -K(\varphi^\flat,\varphi_1,\alpha)$ from the 1st line and $\sqrt{2f}(s^\flat - 1) = K(\varphi^\flat,\varphi_1,\alpha) - K(\varphi_1,\varphi_1,\alpha)$ from the 2nd one. Finally, we have the useful formulae $\sqrt{2f} = K(\varphi_1,\varphi_1,\alpha) - 2K(\varphi^\flat,\varphi_1,\alpha)$ yielding the force explicitly as

$$\boxed{f = \tfrac{1}{2}\left[K(\varphi_1,\varphi_1,\alpha) - 2K(\pi + 2\alpha - \varphi_1,\varphi_1,\alpha)\right]^2} \tag{2.15}$$

and

$$\sqrt{2f}\, s^\flat = -K(\varphi^\flat,\varphi_1,\alpha). \tag{2.16}$$

As we announced in the foregoing section we can now sketch the relations $f = f(\alpha,\varphi_1)$ given in (2.8) for the convex elastica and (2.15), now under the supposition that one flex point exists.

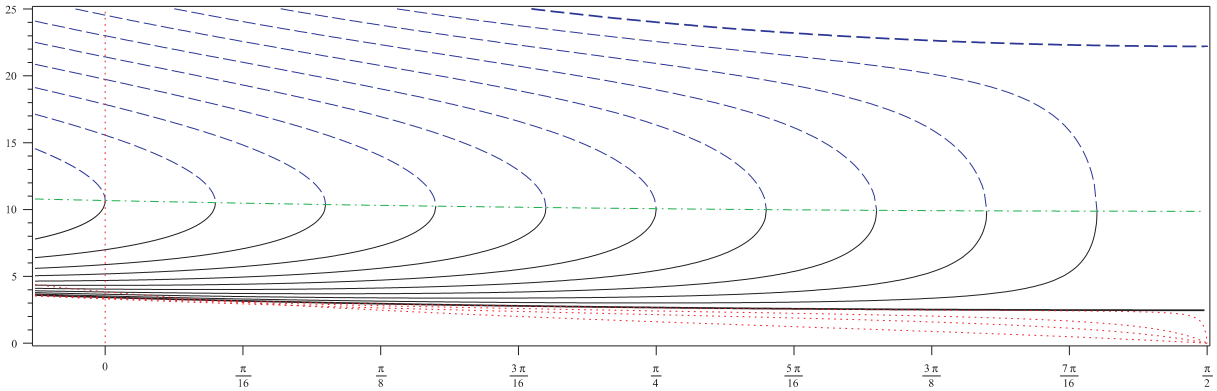

Figure 2: Force f vs. tip slope φ_1 for various α.

In fact, this family of curves deserves a particular interest: given any point (φ_1, f) of the curve "numbered" α, then the triplet (α,φ_1,f) characterizes a unique elastic line through the differential equations (2.3). That means, that this family of curves is a kind of *configuration space* of the Bernoulli rods under consideration.

There are several types of schlicht curves. The bold curves for $\alpha = 0$ (vertical force) end at $\varphi_1 = \frac{\pi}{2}$, with $f = \frac{1}{4}\pi^2$ (lower one: zero flex point) and at $\varphi_1 = \frac{\pi}{2}$ with $f = \frac{9}{4}\pi^2$ (upper one: one flex point), respectively. Evidently, these f-values are just the 1st and 2nd critical buckling load.

The solid curves above come from (2.8), no flex point with $\alpha = -\frac{\pi}{4}(\frac{\pi}{40})0$. Each curve with fixed negative α terminates vertically at $\varphi_{1\alpha} = \frac{\pi}{2} + 2\alpha$, $f_\alpha = 4\mathbb{K}^2(\sin(\frac{\alpha}{2}))$, ($\mathbb{K}(\cdot)$: complete elliptic integral of 1st kind, see Appendix A). These points in the (φ_1, f)-plane mark the border of the theory with convex elastic lines. This becomes obvious if we notice $\kappa\,|_{s=0} = 0$ from (2.6). The geometric locus of these points is the middle dash-dot line. In fact, these points are turning points since they join to the dashed (φ_1, f)-curves given by (2.15), one flex point.

The lowest region in the diagram is filled with (φ_1, f)-curves given by (2.8) with positive α (only few of them shown dotted-lined, they are not of interest in our context).

Being sure that actually there is a flex point and we know α and φ_1 then $\varphi^\flat$, $s^\flat$ and f follow from (2.12), (2.15) and (2.16). Finally, the elastic line can be determined by the procedures **(a)** and **(b)** explained in Subsection 2.1.1.

If we prefer to proceed by the method **(c)** given there, i.e., ODEs (2.3a,b,c) and parameter transformation $s \to \varphi$ now piecewise using (2.11), we come to the following:

$$\varphi = \frac{\pi}{2} \ldots \varphi^\flat : \begin{cases} x = \frac{1}{\sqrt{2f}} \int\limits_{\frac{\pi}{2}}^{\varphi} \cos(t) \left[\sin(t-\alpha) - \sin(\varphi_1 - \alpha)\right]^{-1/2} dt \equiv -X(\varphi), \\ y = \frac{1}{\sqrt{2f}} \int\limits_{\frac{\pi}{2}}^{\varphi} \sin(t) \left[\sin(t-\alpha) - \sin(\varphi_1 - \alpha)\right]^{-1/2} dt \equiv -Y(\varphi), \end{cases}$$

$$\varphi = \varphi^\flat \ldots \varphi_1 : \begin{cases} x - x^\flat = \frac{-1}{\sqrt{2f}} \left(\int\limits_{\varphi^\flat}^{\frac{\pi}{2}} \cos(t) \left[\sin(t-\alpha) - \sin(\varphi_1 - \alpha)\right]^{-1/2} dt \right. \\ \qquad \left. + \int\limits_{\frac{\pi}{2}}^{\varphi} \cos(t) \left[\sin(t-\alpha) - \sin(\varphi_1 - \alpha)\right]^{-1/2} dt \right) \equiv X(\varphi) - X(\varphi^\flat), \\ y - y^\flat = \frac{-1}{\sqrt{2f}} \left(\int\limits_{\varphi^\flat}^{\frac{\pi}{2}} \sin(t) \left[\sin(t-\alpha) - \sin(\varphi_1 - \alpha)\right]^{-1/2} dt \right. \\ \qquad \left. + \int\limits_{\frac{\pi}{2}}^{\varphi} \sin(t) \left[\sin(t-\alpha) - \sin(\varphi_1 - \alpha)\right]^{-1/2} dt \right) \equiv Y(\varphi) - Y(\varphi^\flat). \end{cases}$$

Here $X(\varphi)$, $Y(\varphi)$ abbreviate the evaluable function values $X(\varphi; f, \varphi_1, \alpha)$, $Y(\varphi; f, \varphi_1, \alpha)$ introduced in (2.10). Continuity of the elastic line demands $x^\flat = -X(\varphi^\flat)$, $y^\flat = -Y(\varphi^\flat)$. Hence, we obtain the *representation of the elastic line with one flex point* in analogy to (2.10)

$$\boxed{\begin{aligned} x &= \begin{cases} -X(\varphi; f, \varphi_1, \alpha), & \varphi = \frac{\pi}{2} \ldots \varphi^\flat \\ X(\varphi; f, \varphi_1, \alpha) - 2X(\varphi^\flat; f, \varphi_1, \alpha), & \varphi = \varphi^\flat \ldots \varphi_1 \end{cases}, \\ y &= \begin{cases} -Y(\varphi; f, \varphi_1, \alpha), & \varphi = \frac{\pi}{2} \ldots \varphi^\flat \\ Y(\varphi; f, \varphi_1, \alpha) - 2Y(\varphi^\flat; f, \varphi_1, \alpha), & \varphi = \varphi^\flat \ldots \varphi_1 \end{cases}. \end{aligned}} \tag{2.17}$$

Again, we refer to the Appendix A to find a usable representation by standard elliptic integrals. At this stage we do not worry about the stability of states showing a flex point.
Figure 3 shows two elastic lines both with the same *prescribed* values of α and φ_1, whereas the tip forces f are different since determined from (2.8) and (2.15), respectively.

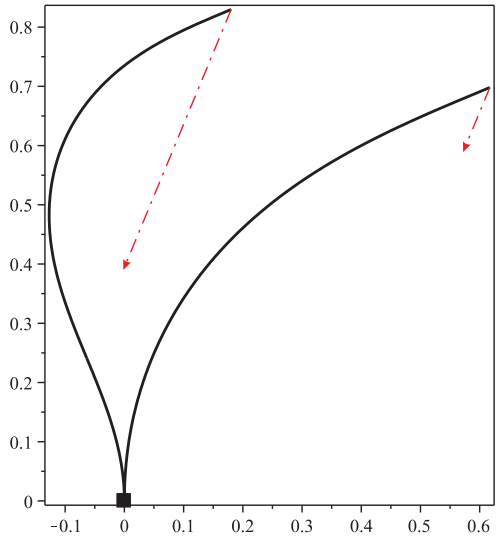

Figure 3: Elastic lines with zero and one flex point, tip forces acting under $\alpha = -\frac{\pi}{8}$, tip slopes prescribed as $\varphi_1 = \frac{1}{2}(\frac{\pi}{2} + 2\alpha)$. Dashed segments represent tip forces $f = 4.72$ and $f = 19.0$.

Remark 2.1. *In Fig. 3 one may notice that the flex point bisects the arc between the two points with slope $\varphi = \frac{\pi}{2}$. This can be proven by means of (2.14).*

3 Vibrissa for surface texture detection

Now we tackle the problem set up at the end of the Section 1 (Introduction): to detect the texture of a surface by means of a vibrissa in passive mode.

3.1 Physical model

Clearly, we use a bending rod to model the vibrissa, and we admit the following confinements of the overall scene.

(a) The object to be scanned is a plane (a straight line in our configuration space $\mathbb{R}^2$);

(b) The vibrissa is originally straight and vertical, its foot is supported by a clamp that is movable along the x-axis;

(c) The to-be-scanned line is horizontal at a level η above the vibrissa foot;

(d) The texture of that line is characterized by *stiction* (Coulomb's "dry friction").

We start the scan process in a configuration with the vibrissa bent right-handed and touching the object under an inclination (tip slope) $\varphi_{10} \in (0, \frac{\pi}{2})$, its foot coordinate is taken as $x_0 = 0$. This configuration is achieved if we choose a level $\eta \in (\underline{\eta}, 1)$, where $\underline{\eta}$ is that tip coordinate y_1 of a convex vibrissa under vertical tip load $\mathbf{f}$ ($\alpha = 0$) which causes the tip slope $\varphi_1 = 0$. From (2.8) and (2.10) we obtain

$$\underline{f} = \tfrac{1}{2}K^2(0,0,0) = 3.4373, \quad \underline{\eta} = Y\left(0; \underline{f}, 0, 0\right) = 0.4569\ .$$

Having chosen any feasible $\eta \in (0.4569, 1)$, then we need the corresponding f and φ_1. For this end, we have to solve the equation

$$Y\left(\varphi_1; \frac{1}{2}K^2\big(\varphi_1, \varphi_1, 0\big), \varphi_1, 0\right) - \eta = 0,$$

for φ_1 and, using the solution $\varphi_{1\eta}$, we obtain

$$f_\eta := \frac{1}{2}\, K^2\left(\varphi_{1\eta}, \varphi_{1\eta}, 0\right).$$

Figure 4 sketches these values versus the altitude η, whereas Fig. 5 shows the elastic lines for $\eta = 0.6$ and $\eta = 0.75$.

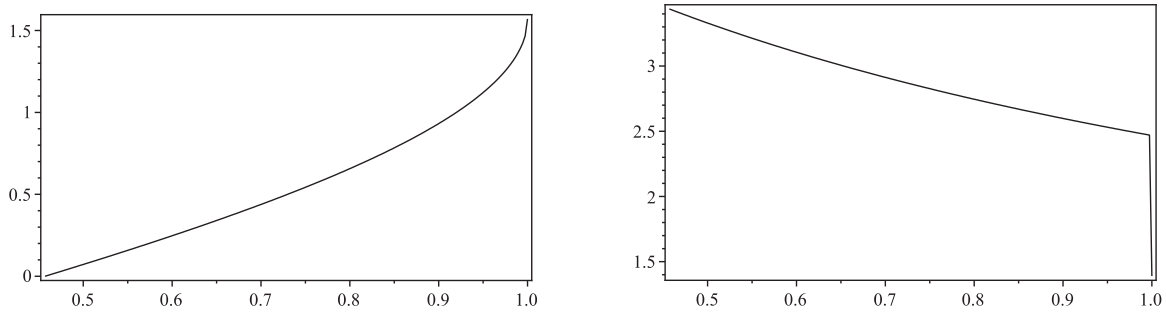

Figure 4: Left: $\varphi_{1\eta}$ vs. η; right: f_η vs. η.

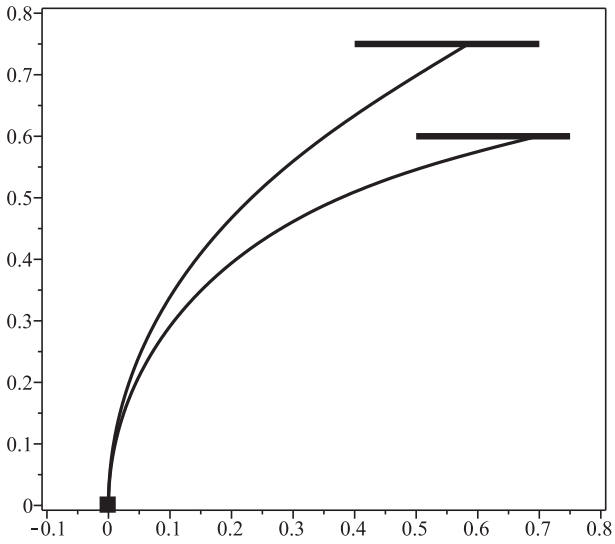

Figure 5: Elastic lines under vertical tip force with two different prescribed tip altitudes η.

Now, the physical procedure to be simulated is as follows:
We displace the vibrissa foot from $x_0 = 0$ to some small $\widetilde{x}_0 > 0$. If the contact was ideal then the vibrissa tip would slide from x_1 to $\widetilde{x}_1 = x_1 + \widetilde{x}_0$ while the tip force $\mathbf{f}$ does not change. However, if there is some "roughness" in the contact region, this becomes apparent by stiction: the tip gets locked by an additional horizontal constraint force acting to the left, i.e., the total tip load $\mathbf{f}$ has got a clock-wise rotation by a certain angle $\alpha < 0$ (maybe accompanied by some change in magnitude). We repeat this step by another foot displacement, again changing the direction of the tip force. The contact point stays at rest as long as the horizontal component of the constraint force, f_x, does not exceed the threshold given by Coulomb's law

$$|f_x| \leq \mu_0 \, |f_y| \, ,$$

where μ_0 is just that stiction coefficient we are aiming at.

If the forces f_x and f_y are under permanent observation (through a measurement device in the foot region) during the process then the violation of Coulomb's relation is noticed by some "bang", and the last measured values yield μ_0. After the tip has slipped forward to a new rest position, the procedure starts anew.

So far about a first experimental way to determine the stiction coefficient μ_0.

3.2 Mathematical model and simulations

In the *mathematical simulation* it seems more convenient to mimic every step in reverse direction: prescribe a negative α and compute the corresponding elastica restricted by $y\,|_{s=1} = \eta$.[1] Running a sequence of steps this way, we end up with the relation $foot\ displacement \to \alpha$. If this is formally known for various η (as far as the computer is willing), then the measurement in experiment can be converted (and simplified) from forces to displacements: $displacement \to \mu = \tan(-\alpha)$. The Coulomb stiction coefficient μ_0, we aim at, shows up in that step where the "bang" takes place.

Clearly, if we start with $\alpha = 0$ (vertical $\mathbf{f}$) then no flex point occurs at first, and the evaluations run according to Subsection 2.1.1 (*phase 0*). But, at some $\alpha < 0$, it may happen that a flex point is born, and the next computing (*phase 1*) has to follow Subsection 2.1.2.

Using MAPLE 15, it appears that passing the turnover point ($\varphi_\alpha = \frac{\pi}{2} + 2\alpha$, $f_\alpha = f(\alpha, \varphi_\alpha)$) is a bit trickish (to choose the right density of the α-sequence and the resolution of equations

[1] Using the toolkit from Subsection 2.1 we have, first of all, a fixed foot at $(0, 0)$ and a displaced tip (x_1, η). Afterwards, a translation has to shift the elastic line to a position with the tip in its starting place.

deserved some caution). Anyway, the *computing process* runs through the following steps. (Every function needed is defined and represented by means of standard functions (see Appendix A) in the preliminaries of the program.)

- Step 0: Choose η, choose some α-sequence $(\alpha_0, \alpha_1, \ldots) \subset [-\frac{\pi}{4}, 0]$, $\alpha_{i+1} < \alpha_i$. For $\alpha = \alpha_0 = 0$ find (φ_{10}, f_0) such that (see (2.10), (2.8)) $Y(\varphi_{10}, f_0, \varphi_{10}, \alpha_0) = \eta$ and $f_0 = \frac{1}{2}K^2(\varphi_{10}, \varphi_{10}, \alpha_0)$.
- Step $n > 0$: For $\alpha = \alpha_n$ find (φ_{1n}, f_n) such that $Y(\varphi_{1n}, f_n, \varphi_{1n}, \alpha_n) = \eta$ and $f_n = \frac{1}{2}K^2(\varphi_{1n}, \varphi_{1n}, \alpha_n)$. Check $\varphi_{1n} < \varphi_{1n-1}$. If $\varphi_{1n} = \frac{\pi}{2} + 2\alpha_n$ then $n =: n_1$: end of no-flex-point phase 0! If $\varphi_{1n_1} = 0$ then stop, else (using tools from Subsection 2.1.2)
- Step $n > n_1$: For $\alpha = \alpha_n$ find (φ_{1n}, f_n) such that (see (2.17), (2.15)) $y\,|_{\varphi=\varphi_{1n}} = \eta$ and $f_n = f(\alpha_n, \varphi_{1n})$ until a computing break occurs (reasons for the latter still unknown).

The results of these steps become apparent by a point sequence $(\varphi_{1n}, f_n)_{n=0,1,\ldots}$ in the (φ_1, f)-plane. The phase 0 part of this sequence obviously terminates in a well-defined turning point $(\varphi_{1n_1}, f_{n_1})$ with $\alpha = \alpha_{n_1}$ such that $f_{n_1} = 4\,\mathbb{K}^2(\sin(\frac{\alpha}{2}))$.

Remark 3.1. *Finally, it turned out that a modification of this procedure is more robust and efficient: Determine, first, the turning point the (φ_1, f)-sequence has to terminate at α solving $Y(\varphi_\alpha, f(\alpha, \varphi_\alpha), \varphi_\alpha, \alpha) = \eta$ where $\varphi_\alpha = \frac{\pi}{2} + 2\alpha$. Then, start with a choice descending φ_1-sequence in $[\varphi_1, \varphi_\alpha]$ and determine for each φ_{1n} the corresponding α_n and $f(\alpha_n, \varphi_{1n})$.*

An example is given in Fig. 6.

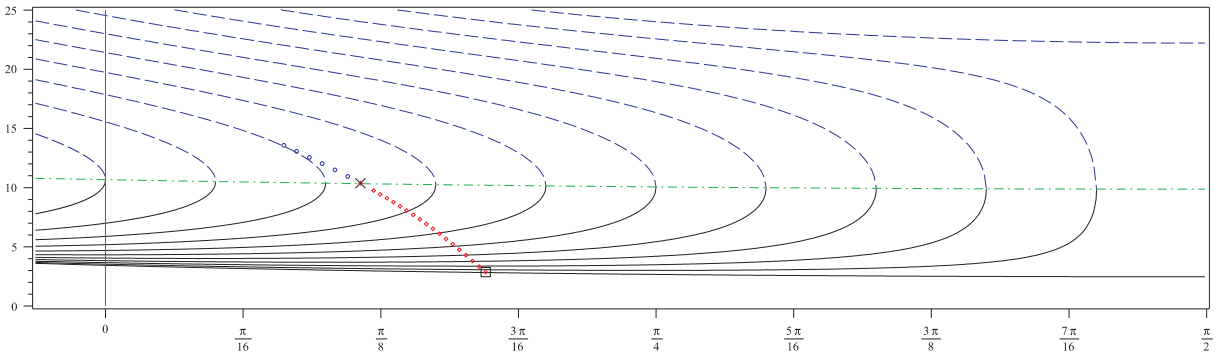

Figure 6: Sequence $(\varphi_{1i}, f_i)_{i=0,1,\ldots}$ for $\eta = 0.75$ (cross: calculated turning point).

The following two figures, Figs. 7 and 8, sketch some of the corresponding elastic lines (dots mark flex points) and the relation of the foot displacement d and $\mu :=| \frac{f_x}{f_y} |=| \tan(\alpha) |$.

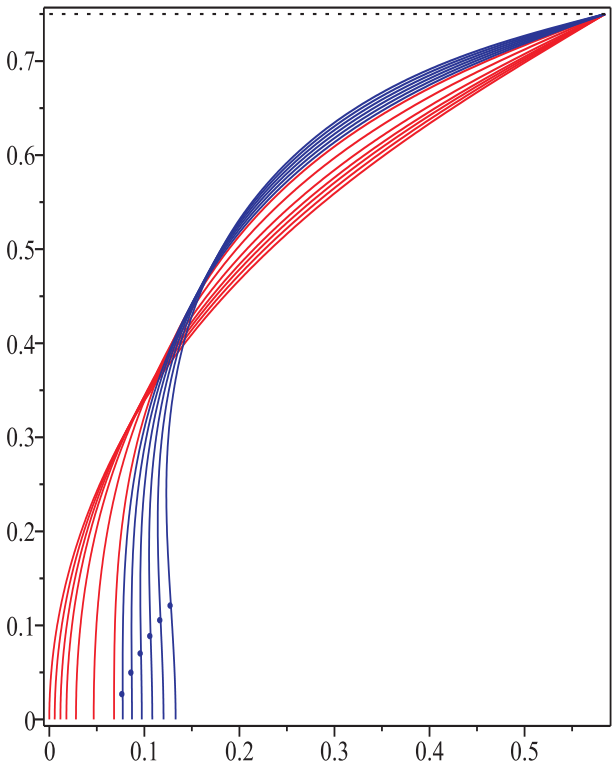

Figure 7: Elastic lines.

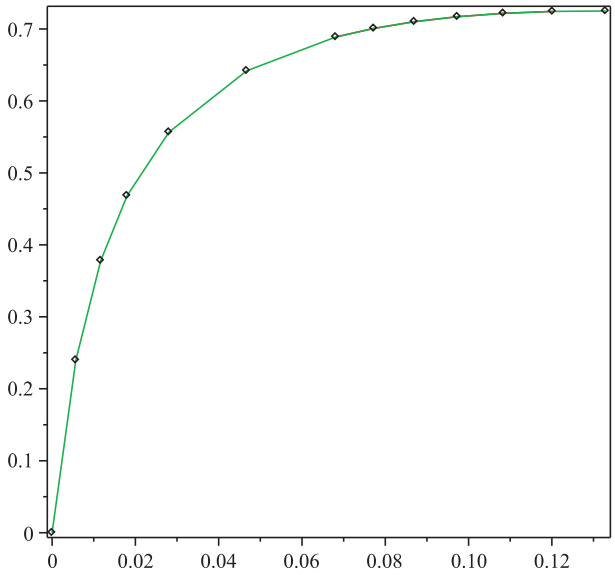

Figure 8: Coefficient μ vs. foot displacement d.

The handling in practice is now this: Run an experiment with $\eta = 0.75$. Aim is at the maximal value of μ - the coefficient μ_0 in Coulomb's law - which marks the roughness of the scanned surface. Experimentally, μ_0 is reached at that (measured) displacement d_0 where a "bang" is observed (tip gets slipping), then μ_0 is obtained from Fig. 8.

Figures 9 to 11 show the analogues for the smaller height $\eta = 0.6$.

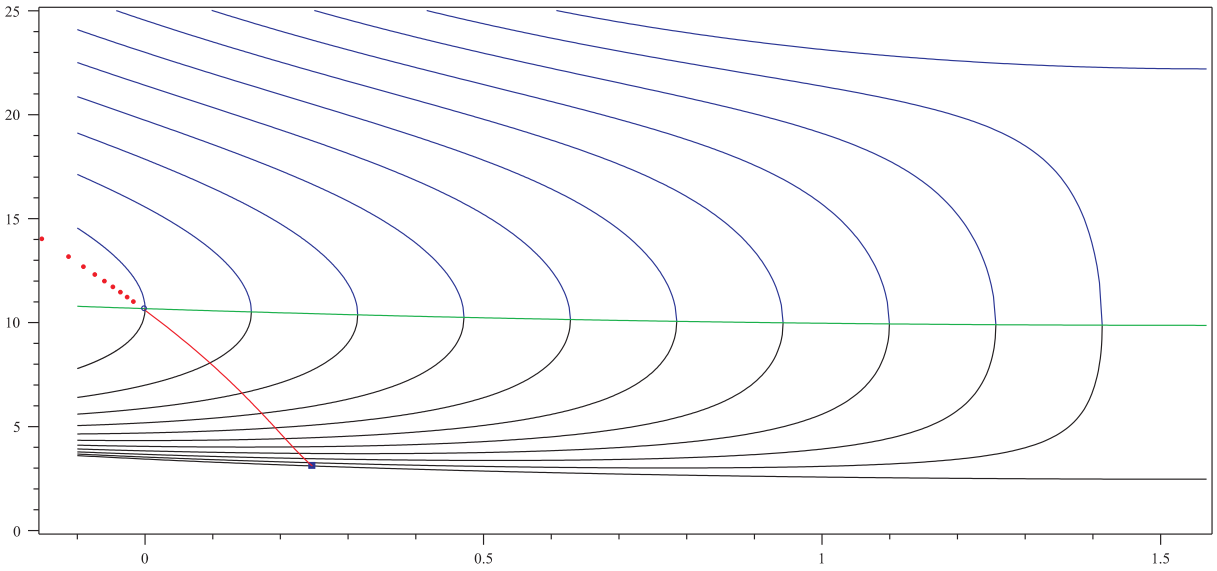

Figure 9: Sequence $(\varphi_{1i}, f_i)_{i=0,1,\ldots}$ for $\eta = 0.6$.

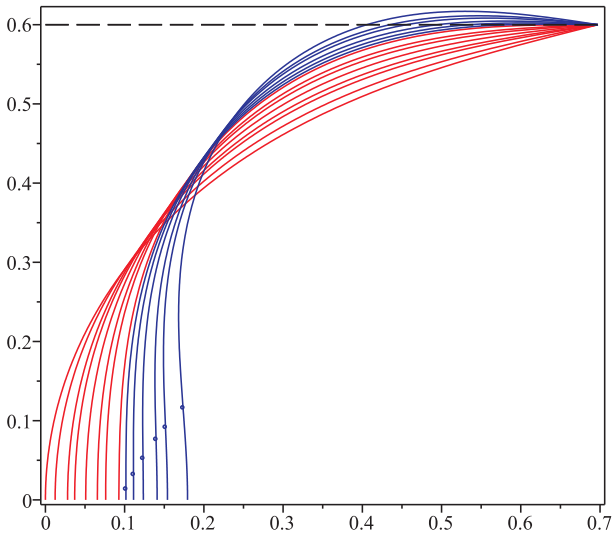

Figure 10: Elastic lines.

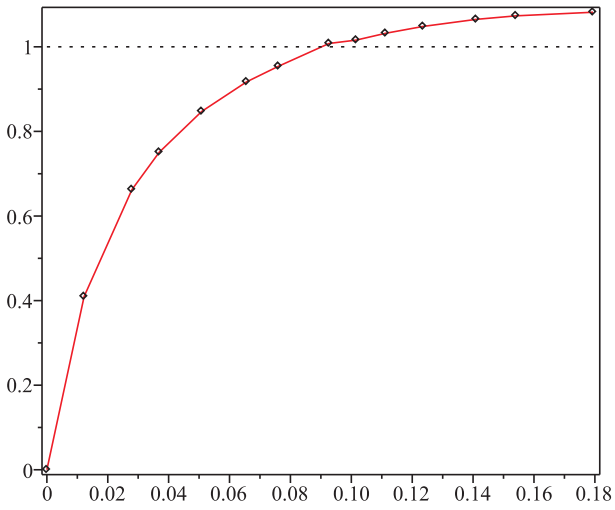

Figure 11: Coefficient μ vs. foot displacement d.

Here, a particular case was met by accident: Figure 9 shows that the no-flex-point phase 0 terminates at $\alpha = -\frac{\pi}{4}$, $\varphi_1 = 0$. Running further steps, then negative φ_1 appear (visible in Fig. 9) which are coupled with an overshooting of the elastic line. This effect is quite correct in the theory of bending rods with tip fixed in $\mathbb{R}^2$.

Precisely, our context needs a stronger theory with a compound constraint

$$\{y(1) = \eta \ \wedge \ y(s) \leq \eta \quad \text{for every} \ \ s \in (0,1)\}$$

instead of solely $y(1) = \eta$. Clearly, the experimental run ends at that step with $\varphi_1 = 0$.

4 Conclusion

The authors would like to understand the foregoing investigations as a first attempt to incorporate stiction into touch problems with vibrissae. The underlying mathematical model admits a far-reaching analytical treatment, this is due to several simplifying assumptions in the physical model:

- the vibrissa is modeled as a bending rod that is originally straight, it has a constant bending stiffness, and it is made of homogeneous Hooke elastic material;
- the vibrissa foot is clamped, its tip is constrained to fixed constant level.

This makes the core of the mathematical model an *autonomous* ordinary differential equation boundary value problem, whose energy integral enables one to present the solution of the total boundary value problem by means of elliptic integrals. So, the numerical exploitation is shifted as far as possible, and final simulations only need evaluation of standard functions. The latter was achieved on the PC by means of MAPLE 15.

Although at first there is no urgent necessity, this way of simulation can be changed (and should be changed to see the effects):

- replace the computer algebra-oriented software MAPLE used for evaluating the analytical expressions by a different, numerical software, as for instance MATLAB;
- use a numerical software from the very beginning, i.e., solve the total boundary value problem numerically (without handling solutions analytically).

The last mentioned way of treating the problem might become unavoidable if the physical model is improved. Notice that the real vibrissa may be non-cylindrical but tapered (diameters of the cross-sections decrease towards the tip), and the original stress-free shape is not a straight line (there is a non-zero pre-curvature $\varkappa_0$ depending on s in general). Then the bending stiffness EI_z is not constant anymore (same effect if E depends on s) and the classical bending relation $\varkappa = m$ turns into $\varkappa - \varkappa_0(s) = b(s)m$, where, after normalization, b represents the reciprocal bending stiffness. The differential equation (2.3,d) then writes

$$\varkappa' - \frac{b'}{b}\varkappa = b\,m + \left(\varkappa_0' - \frac{b'}{b}\varkappa_0\right),$$

it shows up as *non-autonomous* (exceptional case: constant stiffness, $b' = 0$, and circular pre-curvature: $\varkappa_0' = 0$), and it demands a more complicated treatment. This must be accepted if in particular the effects of tapering and pre-curving on the behavior of the vibrissa are to be explored.

Another improvement relates to the vibrissa support. The real vibrissa is rooted in the follicle-sinus complex with its various biological devices. So, the least improvement towards mimicking the follicle-sinus complex would be to replace the clamp with a viscoelastic support which simultaneously could serve for certain control tasks.

Assume that these effects are sufficiently well known or not of interest then another kind of model improvement is to replace the straight horizontal tip constraint by any inclined or curved one. Thereby, the model comes closer to the scenario in object scan but now dropping the assumption of ideal touch and instead allow for roughness of the contacting surfaces.

In order to validate the presented theory (and its hopefully coming improved versions) a measuring device for the investigation of hardware macro models is currently in statu nascendi. At the Department of Technical Mechanics (Ilmenau University of Technology, Germany), experiments are to start in next future.

Possibly, this gives rise to establish a dynamical theory of vibrissae in stick-slip motion (thereby enlightening also the dark "bang" from above).

This paper contributes to the DFG-supported research project "Technical, non-visual characterization of substrate contact using carpal vibrissae as a biological model", [Schmidt et al. 2014], (TU Ilmenau: Departments Technical Mechanics & Biomechatronics; FSU Jena: Institute of Systematic Zoology and Evolutionary Biology with Phyletic Museum).

A Elliptic integrals

Representations by standard elliptic integrals are given for the most frequently appearing functions in the theory.

The standard elliptic integrals, in MAPLE to be called by 'EllipticF', etc., are the following.
Elliptic integral of 1st kind:

$$\mathbb{F}(z,k) := \int_0^z \frac{1}{\sqrt{1-t^2}\sqrt{1-k^2t^2}}dt,\ (k<1).$$

Complete elliptic integral of 1st kind:

$$\mathbb{K}(k) := \mathbb{F}(1,k).$$

Elliptic integral of 2nd kind:

$$\mathbb{E}(z,k) := \int_0^z \sqrt{\frac{1-k^2t^2}{1-t^2}}dt,\ (k<1).$$

(z: *argument*, k: *module*).

We sketch some reformulations of relevant integrals encountered in the foregoing sections and give their acceptable final form. Most frequently we met the integrals

$$\int_{\pi/2}^{\varphi} [\sin(\tau-\alpha)-\sin(u)]^{-1/2}\,d\tau \text{ and } \int_{\pi/2}^{\varphi} \begin{matrix}\sin(\tau)\\ \cos(\tau)\end{matrix}\ [\sin(\tau-\alpha)-\sin(u)]^{-1/2}\,d\tau$$

with $u := \varphi_1 - \alpha$. We introduce the following abbreviations

$$\begin{aligned}
I_1(x,u) &:= \int_{\pi/2}^{x} [\sin(\tau)-\sin(u)]^{-1/2}\,d\tau,\\
I_2(x,u) &:= \int_{\pi/2}^{x} [\sin(\tau)-\sin(u)]^{1/2}\,d\tau,\\
I_3(x,u) &:= \int_{\pi/2}^{x} \sin(\tau)\ [\sin(\tau)-\sin(u)]^{-1/2}\,d\tau,\\
I_4(x,u) &:= \int_{\pi/2}^{x} \cos(\tau)\ [\sin(\tau)-\sin(u)]^{-1/2}\,d\tau.
\end{aligned}$$

Applying transformations like this:

$$\begin{aligned}
I_1 &= \int_{\pi/2}^{x} \left[\cos\left(\tau-\tfrac{\pi}{2}\right)-\sin(u)\right]^{-1/2} d\tau = \int_{0}^{x-\frac{\pi}{2}} \left[\cos(\sigma)-\sin(u)\right]^{-1/2} d\sigma \\
&= \int_{0}^{x-\frac{\pi}{2}} \left[1-2\sin^2\left(\tfrac{\sigma}{2}\right)-\sin(u)\right]^{-1/2} d\sigma, \qquad \text{let } k(u) := \tfrac{1}{\sqrt{2}}\sqrt{1-\sin(u)}, \\
&= \tfrac{1}{\sqrt{2}k(u)} \int_{0}^{x-\frac{\pi}{2}} \left[1-\tfrac{1}{k(u)^2}\sin^2\left(\tfrac{\sigma}{2}\right)\right]^{-1/2} d\sigma, \qquad \text{substitution: } \sin\left(\tfrac{\sigma}{2}\right) = k(u)\cdot z, \\
&= \sqrt{2} \int_{0}^{\frac{1}{k}\sin\left(\frac{x}{2}-\frac{\pi}{4}\right)} \left[\left(1-z^2\right)\left(1-k^2z^2\right)\right]^{-1/2} dz,
\end{aligned}$$

we obtain the auxiliary function

$$\boxed{\begin{array}{l} I_1(x,u) = \sqrt{2}\,\mathbb{F}\left(\tfrac{1}{k(u)}\sin\left(\tfrac{x}{2}-\tfrac{\pi}{4}\right), k(u)\right) \\ \text{with module } k(u) = \sqrt{\tfrac{1}{2}\left(1-\sin(u)\right)}. \end{array}}$$

Similarly we get

$$\boxed{I_2(x,u) = 2\sqrt{2}\left\{\mathbb{E}\left(\tfrac{1}{k(u)}\sin\left(\tfrac{x}{2}-\tfrac{\pi}{4}\right), k(u)\right) - \left(1-k(u)^2\right)\mathbb{F}\left(\tfrac{1}{k(u)}\sin\left(\tfrac{x}{2}-\tfrac{\pi}{4}\right), k(u)\right)\right\}.}$$

Rewriting

$$\begin{aligned}
I_3 &= \int_{\frac{\pi}{2}}^{x} \left\{\sin(u)+\sin(\tau)-\sin(u)\right\}\left[\sin(\tau)-\sin(u)\right]^{-1/2} d\tau, \\
I_4 &= \int_{\frac{\pi}{2}}^{x} 2\,\tfrac{d}{d\tau}\left\{\left[\sin(\tau)-\sin(u)\right]^{1/2}\right\} d\tau,
\end{aligned}$$

we find

$$\boxed{\begin{array}{l} I_3(x,u) = \sin(u)\cdot I_1(x,u) + I_2(x,u), \\ I_4(x,u) = 2\left\{\sqrt{\sin(x)-\sin(u)} - \sqrt{1-\sin(u)}\right\}. \end{array}}$$

In relation to the elastica coordinate Y, there appears

$$J_s(\varphi,\varphi_1,\alpha) := \int_{\frac{\pi}{2}}^{\varphi} \sin(t)\left[\sin(t-\alpha)-\sin\left(\varphi_1-\alpha\right)\right]^{-1/2} dt$$

and analogously $J_c := \int \cos(t)[\ldots]^{-1/2}dt$ for X. Putting $t = \tau+\alpha$, and using addition theorems for $\sin(\tau+\alpha)$, and $\cos(\tau+\alpha)$, the J integrals show up as linear combinations of I_3 and I_4.

Altogether, we have the following comfortable way to handle the relevant objects of the theory:

$$\boxed{\begin{array}{l} K(\varphi,\varphi_1,\alpha) = -I_1(\varphi-\alpha,\varphi_1-\alpha) + I_1\left(\tfrac{\pi}{2}-\alpha,\varphi_1-\alpha\right), \\ \sqrt{2f}\cdot X(\varphi;f,\varphi_1,\alpha) = \sin(\alpha)\left[I_3(\varphi-\alpha,\varphi_1-\alpha) - I_3\left(\tfrac{\pi}{2}-\alpha,\varphi_1-\alpha\right)\right] \\ \qquad\qquad - \cos(\alpha)\left[I_4(\varphi-\alpha,\varphi_1-\alpha) - I_4\left(\tfrac{\pi}{2}-\alpha,\varphi_1-\alpha\right)\right], \\ \sqrt{2f}\cdot Y(\varphi;f,\varphi_1,\alpha) = -\cos(\alpha)\left[I_3(\varphi-\alpha,\varphi_1-\alpha) - I_3\left(\tfrac{\pi}{2}-\alpha,\varphi_1-\alpha\right)\right] \\ \qquad\qquad - \sin(\alpha)\left[I_4(\varphi-\alpha,\varphi_1-\alpha) - I_4\left(\tfrac{\pi}{2}-\alpha,\varphi_1-\alpha\right)\right], \end{array}}$$

where I_1, I_2, I_3, I_4 have to be taken from above. Regarding internal computer peculiarities it is advisable to use real parts $\mathrm{Re}(\cdot)$ explicitly and compute with high precision (say, $Digits := 25$).

B Supplement

It is unquestionable that scientists from different branches come along with different concrete interests for natural objects, their structure, interconnections and interactions, and they show a preference for different investigation methods. Our current research group may serve as a striking example.

Although there is one common general research object - bio-inspired sensors - several scientific branches are present: biology, zoology, medicine, mechanics, mathematics.

Certainly, it is the business of biologists and zoologists to investigate natural objects (e.g., sensory organs like vibrissae) in a maximum of details: geometry, material, behavior under external influences, structure and mode of operation of the supporting elements like the follicle-sine complex (FSC).This task blows up due to the multiple forms of vibrissae, distinguished by their place on the surface of a living organism (mystacial v.: snout region, carpal v.: foot region, as examples) in connection with various purposes (object perception quite near or afar). This raises questions: which structure (created through evolution) makes the vibrissa optimally fit for its task? And which internal processes are the very reason for this fitness? It may be true that the answers to these questions are primarily sought by means of both *in vivo* and *in vitro* observations and measuring. Their results then lead to hypotheses and further on to theories which describe structure and functioning of a group of natural objects.

Co-operating engineering scientists are primarily interested in the *principles* of structure and functioning with the final aim to design an artificial object that (under choice aspects) comes close to the live paragon. For this end they take up the results gained by the life scientists as the basis of their own work that specifically uses techniques from technology, physics, and mathematics.

And this is just the principle of bionics: *See the nature and adopt evolutionary achievements to technology.*

The overwhelming complexity of natural objects excludes, from the very beginning, the investigation of such objects as a whole, i.e., as they show up with all their details. Any investigation has to focus on a *model* of the object, and this means, take the (possibly incomplete) image of the object presented by the observing scientists (biologists, zoologists), dissect this image and take away all pieces of (actual or guessed) non-interest. The rest then forms a *virtual object*, which all considerations to come have to be concentrated on.

Next, this virtual object must be described by means of physical terms, this description represents a *physical model* of the natural object. Finally, applying corresponding physical theories and turning physical terms into adequate mathematical ones, a *mathematical model* of the natural object has appeared. As a rule, this shows up as a system of constants and variables, combined by equations of any kind. Possibly, based on such models, engineers could design a (preliminary) *hardware model* to be used for demonstration or measuring.

All these steps should strictly follow this general guide in modeling: *Make the model as simple as possible* (to enable a thorough analysis) *and as comprehensive and complicated as necessary* (to capture all important items). The extent of performing these claims obviously depends on objective necessities and subjective abilities to master the coming steps. (To quote Albert Einstein: “Everything should be made as simple as possible, but no simpler”.)

The analysis of the mathematical model consists of the following items:

1) to find general or particular solutions of the equations,

2) to study these solutions under different feasible values of system parameters,

3) to compare these simulation results with empirical results from measurements at a hardware physical model or at an original object.

As a rule, this comparison discloses certain deviations in properties and behavior, throwing a light on the quality of the actual model. It must be seen as the normal case that an improvement of the model should make sense or even shows up as unavoidable. Thereby, a natural iteration process has been opened: object→model→comparison→improvement→new model→... Regrettably, most improvements imply a complication of the mathematical model that frequently enforces new methods for treatment. The worst case is, of course, that in some step the comparison definitely shows the model as unusable.

Concluding, a glance to an example from current research:

(1) Object: vibrissa (any kind).

(2) Physical model 1: straight slender rod, foot clamped, tip free, force at tip.

(3) Mathematical model 1: Euler-Bernoulli bending rod, cylindrical, elastic, differential boundary value problems;
solution: a) analytical expressions, PC-evaluation;
b) a-priori numerical software.

(4) Comparison with object: vibrissa tapered, pre-curved, hollow, no clamp.

(5) Improvement: add tapering (how?), pre-curvature (which?), viscoelastic support.

(6) Mathematical model 2: DEs no more autonomous, only solution b).

(7) Compare to results **(3)**: which effects **(5)** on sensitivity, natural frequencies, ...?

It is desirable and useful to start with a mathematical model 1 that admits solutions (e.g., of differential equations) in closed form ("formulas"). These could enable one to exhibit, qualitatively and without numerical expense, the effects of parameter variations. This knowledge may then be utilizable in setting up and running computer software needed for improved models.

References

[Behn 2014] Behn, C. (2014): Modeling, Analysis and Control of Mechanoreceptors with Adaptive Features, in *Informatics in Control, Automation and Robotics Lecture Notes in Electrical Engineering (LNEE)* **325**, J.-L. Ferrier et al. (eds.), Springer, pp. 349–366, DOI 10.1007/978-3-319-10891-9-20

[Behn and Steigenberger 2009] Behn, C.; Steigenberger, J. (2009): Improved Adaptive Controllers For Sensory Systems - First Attempts; in *Modeling, Simulation and Control of Nonlinear Engineering Dynamical Systems*, Editor J. Awrejcewicz, Springer, Amsterdam, pp. 161–178.

[Carl et al. 2012] Carl, K.; Hild, W.; Mämpel, J.; Schilling, C.; Uhlig, R.; Witte, H. (2012): Characterization of statical properties of rat's whisker system; *IEEE Sensors Journal* **12**(2), pp. 340–349.

[Clements and Rahn 2006] Clements, T. N.; Rahn, C. D. (2006): Three-dimensional contact imaging with an actuated whisker; *IEEE Transactions on Robotics* **22**(4), pp. 844–848 (short papers).

[Schmidt et al. 2014] Schmidt, M.; Witte, H.; Zimmermann, K.; Niederschuh, S.; Helbig, T.; Voges, D.; Husung, I.; Volkova, T.; Will, C.; Behn, C.; Steigenberger, J.; Klauer, G. (2014): Technical, non-visual characterization of substrate contact using carpal vibrissae as a biological model: an overview; in *Proceedings 58th Internationales Wissenschaftliches Kolloquium*, Ilmenau (Germany), September 2014, URN (paper): urn:nbn:de:gbv:ilm1-2014iwk-175:8

[Scholz and Rahn 2004] Scholz, G.; Rahn, C. D. (2004): Profile Sensing With an Actuated Whisker; *IEEE Transactions on Robotics and Automation* **20**, pp. 124–127.

[Voges et al. 2012] Voges, D.; Carl, K.; Klauer, G.; Uhlig, R.; Behn, C.; Schilling, C.; Witte, H. (2012): Structural characterisation of the whisker system of the rat; *IEEE Sensors Journal* **12**(2), pp. 332–339.

[Will 2013] Will, C. (2013): Anwendung nichtlinearer Biegetheorie auf elastische Balken zur Objektabtastung am Beispiel passiver Vibrissen mit unterschiedlicher Lagerung; Master thesis, Dept. of Technical Mechanics, Ilmenau University of Technology, 2013.

[Will et al. 2014a] Will, C.; Steigenberger, J; Behn, C. (2014): Object Contour Reconstruction Using Bio-inspired Sensors; in *Proceedings 11th International Conference on Informatics in Control, Automation and Robotics (ICINCO 2014)*, Vienna (Austria), September 2014, pp. 459-467, SciTePress, ISBN: 978-989-758-039-0, DOI: 10.5220/0005018004590467

[Will et al. 2014b] Will, C.; Steigenberger, J; Behn, C. (2014): Quasi-static object scanning using technical vibrissae; in *Proceedings 58th Internationales Wissenschaftliches Kolloquium*, Ilmenau (Germany), September 2014, URN (paper): urn:nbn:de:gbv:ilm1-2014iwk-015:5